6

Iron-dominant transverse fields

In the previous two chapters, we have been discussing transverse field magnets where the field shape is controlled by the distribution of the conductors. When iron was present, it served mainly to enhance the strength of the field produced by the conductors. In this chapter, we examine transverse field magnets where the primary roles of the conductor and the iron are reversed. Here the shape of the field is determined by the shape of the iron surface and the conductors are used to excite the field in the iron.[1, 2] In addition, the iron reduces the reluctance in the magnetic circuit, allowing a larger useful field for a given number of amp-turns from the conductor. These types of magnets typically have a maximum field less than 2 T, so that iron saturation effects do not destroy the field quality. We will mainly be concerned with the calculation of the magnetic fields and do not consider the many engineering considerations necessary to actually build magnets of this type.

6.1 Ideal multipole magnets

If the permeability of the iron is very large ($\mu_r \sim 1000$), it is a useful approximation to assume that μ_r is infinite. In that case, the magnetic flux density B must be perpendicular to the iron surface. The shape of the iron surface in the transverse plane coincides with an equipotential line for the scalar potential. Then, since the equipotential lines of the real and imaginary parts of the complex potential W are orthogonal, the magnetic field follows from the equipotential lines for the vector potential. Each positive pole of the magnet acts like a source of magnetic field, while the negative poles act like a sink where the magnetic field returns back into the iron.

The shape of the iron pole piece for an ideal $2n$-multipole magnet is determined by the complex potential for the multipole, which can be found from conformal mapping to have the form
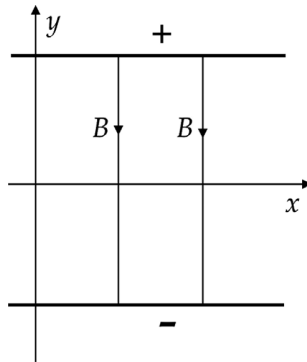
150

Figure 6.1 Iron surfaces and field lines in a dipole magnet.

$$W(z) = c_n z^n$$
$$= c_n \, r^n e^{in\theta},$$

where the constant c_n gives the strength of the potential. The magnetic field for the ideal multipole is given by

$$B^* = i \, \frac{dW}{dz}$$
$$= i \, n \, c_n z^{n-1}.$$

The simplest example of an ideal multipole is the dipole ($n = 1$), which has the complex potential

$$W = c_1 z$$
$$= c_1(x + i \, y).$$

Figure 6.1 illustrates the iron surface and the lines of magnetic field for a dipole magnet. The dipole has two poles with opposite polarity. Taking the real and imaginary parts of W, the vector and scalar potentials are

$$A_z = c_1 \, x$$
$$\mu_0 V_m = c_1 \, y.$$

We see that the iron surface is given by the equipotential

$$c_1 \, y = h,$$

where the constant h identifies a particular surface. The vector potential is given by the equipotential
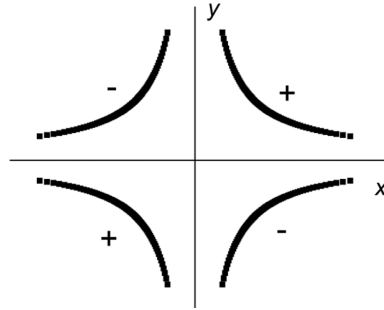
$$c_1 \, x = k,$$

Figure 6.2 Iron surface of an ideal quadrupole, ignoring the asymptotic tails.

where the constant k identifies a particular equipotential line. The magnetic field for the dipole is

$$B_y = -\frac{\partial A_z}{\partial x} = -c_1,$$

which is a constant.

The iron surfaces for higher order ideal multipoles can be found in a similar manner. The ideal quadrupole ($n = 2$) has

$$W = c_2 z^2 \ = c_2(x^2 - y^2 + 2\,i\,x\,y)$$
$$A_z = c_2(x^2 - y^2)$$
$$\mu_0 V_m = 2c_2 x\,y.$$

The iron surface for the ideal quadrupole is the hyperbola

$$x\,y = \frac{h}{2c_2},$$

as shown in Figure 6.2. In polar coordinates, we can write the equation of the hyperbolic surface as

$$r^2 \sin 2\theta = a^2,$$

where a is the radius to the center of a pole and θ is measured from the positive x axis. There are four poles around the perimeter of the magnet that alternate in polarity. The surface hyperbola for a normal quadrupole has asymptotes along the x and y axes. The field components inside the aperture are

$$B_x = -2c_2 y$$
$$B_y = -2c_2 x.$$

The vertical field on the midplane varies linearly across the aperture and is an example of a gradient field.

The symmetry properties of a magnet are determined by the symmetry of the poles. In an ideal normal $2N$-multipole, the poles are located at the azimuthal angles

$$\phi_k = (2k - 1)\frac{\pi}{2N}, \qquad k = 1, 2, \ldots, 2N \tag{6.1}$$

The polarities of the poles alternate in direction. The spacing between the poles is π/N.

6.2 Approximate multipole configurations

It is not possible to build an ideal multipole magnet because the equipotential surfaces extend to infinity. Thus one is faced with approximating the ideal surface as well as possible to meet the field quality requirements for the magnet. Any approximation leads to the presence of additional allowed multipoles. The strength of the normal multipoles are proportional to $\cos \phi_k$. The conductor must be wound around the poles in such a way that the polarities of adjacent poles are in opposite directions. In order to get the poles to alternate in sign, we need

$$\cos\left(\phi_k + \frac{\pi}{N}\right) = -\cos \phi_k.$$

This is the same requirement that we saw in Section 4.6 for current distributions, so the allowed multipole components m are again given by

$$m = N(2n + 1), \qquad n = 0, 1, 2, \ldots$$

Halbach has described methods for determining the effects on the multipole coefficients of iron saturation and perturbations in the fabrication or construction of iron-dominated magnets.[3, 4] These methods involve determining the effect of the perturbation on the scalar potential associated with the pole surface. Among the effects he considers are azimuthal and radial displacements of the poles and modifications in the shape of the pole surface. For example, the addition of an iron shim with thickness profile $h(\phi)$ modifies the unperturbed scalar potential approximately by

$$\delta V_m \approx -h(\phi) H_r(\phi),$$

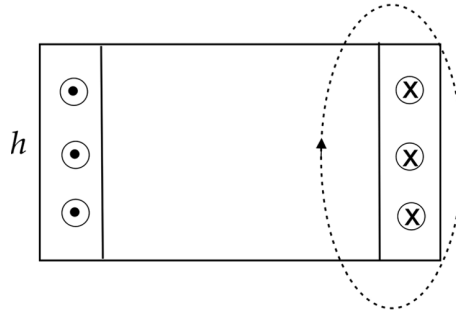where $H_r(\phi)$ is the field on the unperturbed surface.

Figure 6.3 Window frame dipole.

6.3 Dipole configurations

Dipole magnets are commonly used to bend charged particle beams and for experiments requiring a uniform field.[5] The *window frame* dipole, shown in Figure 6.3, is a common configuration.[2, 6, 7] The coils approximate two parallel infinite current sheets, which we saw in Equation 4.33 produces a uniform vertical field. In the window-frame approximation, the field is very uniform across the aperture up to the vicinity of the coils. The field inside the coils falls off approximately linearly, reaching zero at the outer edge of the coils. If we look at the Ampère law around the dotted path indicated in Figure 6.3, we find that

$$NI = \int \overrightarrow{H} \cdot \overrightarrow{dl}$$

$$= \frac{B_0 h}{\mu_0} + \frac{B_0 L_{iron}}{\mu}, \tag{6.2}$$

where NI is the number of amp-turns in the coil, B_0 is the field on the midplane at the center of the aperture, h is the gap between the iron boundaries, and L_{iron} is the path length in the iron. Since $\mu \gg \mu_0$ and the typical path length in the iron is at most a few times greater than the gap, we have

$$\frac{h}{\mu_0} \gg \frac{L_{iron}}{\mu}.$$

The field produced by a window frame dipole is then

$$B_0 \simeq \frac{\mu_0 NI}{h}. \tag{6.3}$$

Note that the field strength is inversely proportional to the size of the gap.
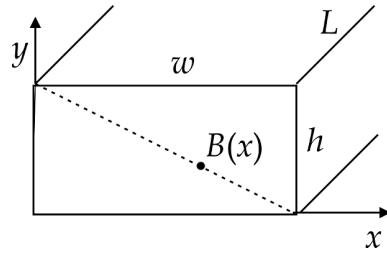
Figure 6.4 Cross-section through a dipole coil. The aperture of the magnet is located at negative *x* in this figure.

For finite permeability, the iron will undergo saturation at high field strengths, the second term in Equation 6.2 may no longer be negligible, and the field in the gap will be smaller than indicated by Equation 6.3. The field is lower at the center of the magnet compared to the field at the edges. This creates a small positive sextupole component in the field. Increasing the width of the pole beyond the useful aperture can improve the field quality.

Figure 6.4 shows a cross-section through one of the coils. The force on the conductor is

$$\overrightarrow{F} = \int \overrightarrow{J} \times \overrightarrow{B} \; dV.$$

The current density can be written as

$$J = \frac{NI}{wh} = \frac{B_0}{\mu_0 w}.$$

Assuming the field falls off linearly across the coil

$$B(x) = B_0 \; \frac{x}{w}$$

and using

$$dV = hL \; dx,$$

we can write [1]

$$F = \frac{B_0^2 \, hL}{\mu_0 \, w^2} \int_0^w x \; dx$$
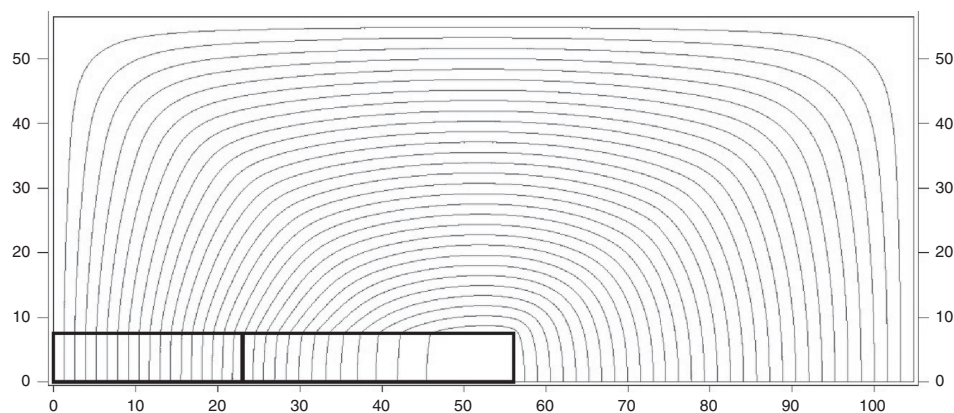
$$= \frac{B_0^2 \, hL}{2 \, \mu_0}.$$

Figure 6.5 POISSON model of a window frame dipole. The dimensions are in centimeters.

Thus the force per unit length acting on the coil is

$$\frac{F}{L} = \frac{B_0^2 \, h}{2\mu_0}$$

and the transverse pressure is

$$P = \frac{B_0^2}{2\mu_0}.$$

Field calculations involving finite permeability iron have to be done using computer programs. Figure 6.5 shows a model[1] of a window frame dipole made with the program POISSON.[2] This figure shows one quarter of the cross-section of the magnet. The box in the lower left corner is an air region, which is the useful aperture in the magnet. The box to the right of the aperture is the conductor region. The remaining region is assumed here to be made of 1010 alloy steel. The contour lines show the direction of the magnetic field, which are vertical and fairly uniform in the aperture. POISSON breaks the iron into a large grid of points where the vector potential is computed. The relative permeability at each grid point is determined from a *B-H* curve. The one used here has a maximum μ_r value of 2,755. The program produces a self-consistent solution of Maxwell's equations. Table 6.1 summarizes the results for three values of the field B_0 at the center of the aperture. The second column shows the minimum value of the relative permeability

---

[1] This is a model of the 18D72 bending magnet that was built at Brookhaven National Laboratory.
[2] We will discuss the POISSON program in more detail in Chapter 11.

Table 6.1 *Summary of POISSON calculations for the window frame dipole*

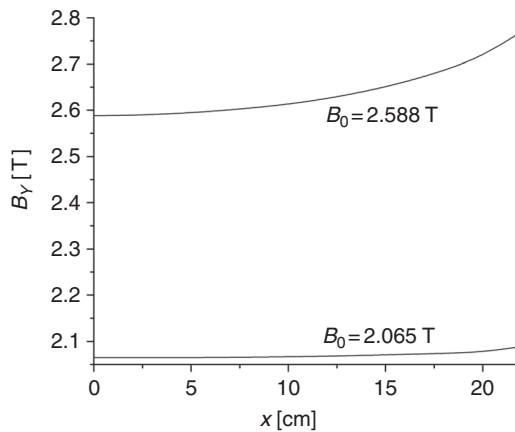| B_0 [T]	Minimum μ_r	$x_{0.001}$ [cm]	F_3
1.56	65	21.2	$3.5\ 10^{-5}$
2.07	13	9.3	$4.0\ 10^{-4}$
2.59	4	3.0	$3.1\ 10^{-3}$

Figure 6.6 Magnetic field along the midplane aperture for the window frame dipole.

at any of the iron grid points. This quantity depends on the field strength in the iron and becomes smaller as the iron saturates at higher fields.

The third column shows the half-width of the good field region, defined here as the distance at which the field exceeds B_0 by more than 10^{-3} T. The last column shows the fractional contribution of the sextupole compared to the dipole contribution to the field. The strength of the field across the half-aperture is shown in Figure 6.6 for the two higher values of B_0. The field is smallest at the center of the aperture and grows as it approaches the conductor.

Another common dipole configuration is the *H*-dipole,[2, 6, 7] shown in Figure 6.7. The coils are recessed and hidden from direct view of the useful part of the magnet aperture. This makes the field less sensitive to errors in the coil location. The field is not as uniform as that in the window frame configuration. The error multipoles in a fixed, useful aperture decrease exponentially with increasing pole width. The iron near the edge of the pole is the first area that exhibits saturation. The good field region can also be extended by adding or subtracting material at the outer edges of the pole, rounding the corners, or by
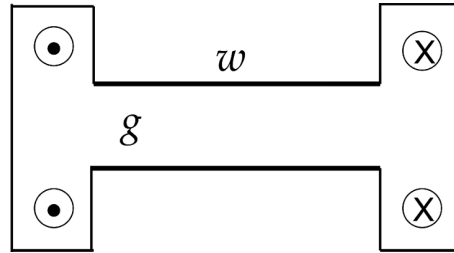
Figure 6.7 Cross-section of an *H*-dipole.

tapering the side edge of the iron. Leakage flux, which circulates around the conductors, can also cause saturation in the iron near the coils, so the magnetic field in the pole piece is maximum at the center of the pole. This creates a negative sextupole component in the field in the aperture.

The effective width of the field is $\approx w + g$. This causes the flux from the midplane to get squeezed going into the poles,

$$wB_{pole} \approx (w + g)B_0,$$

where B_0 is the field on the midplane at the center of the aperture. The field on the pole is then

$$B_{pole} \approx \left(1 + \frac{g}{w}\right)B_0.$$

The *H*-dipole has good field quality and mechanical stability. Simple racetrack-shaped coils can be used to excite the field in the iron.

The *C*-dipole, shown in Figure 6.8, is a configuration that allows good access to the magnet aperture from the side.[2, 6] The field in the iron can be excited with simple racetrack coils. However, the requirement for accessibility leads to a number of disadvantages. The necessary volume of the iron yoke is larger than for an *H*-dipole. There may be considerable leakage flux surrounding the conductors. The asymmetry in the yoke makes the mechanical stability worse. At high field levels, the attractive force between the poles can be quite large. Shims may be required at the edges of the poles to get acceptable field quality. There is a nonuniform magnetic field across the aperture, although this may be a desirable feature for applications that require a gradient field component. The field is smaller on the outside side of the gap than on the inside. The lack of left-right symmetry allows even harmonics to also be present in the field between the pole pieces. The fringe fields between the pole pieces extend outward by about a gap length on both sides of the pole pieces.
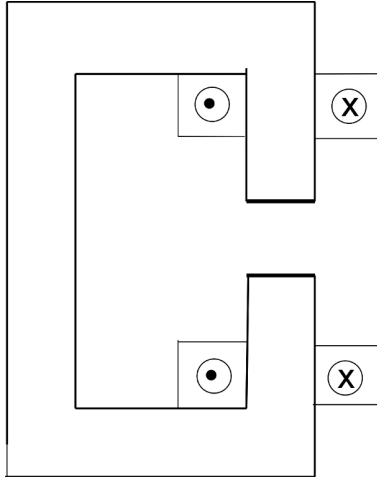
Figure 6.8 Cross-section of a *C*-dipole.

The *effective length* of a dipole, taking into account its end windings, is

$$L_{eff} = \frac{1}{B_0} \int_{-\infty}^{\infty} B(z)\, dz$$
$$\simeq L_{iron} + h,$$

(6.4)

where B_0 is the dipole strength in the center of the magnet. The quantity h is a length proportional to the aperture of the dipole, which takes into account the fringe field extending beyond the iron.

Conformal mapping techniques have been used to improve the modelling of the fringe field from dipole magnets.[8] Maps were used to transform the field from single and double-sided pole pieces with a uniform gap to the upper half of the complex plane.

6.4 Quadrupole configurations

Quadrupole magnets are frequently used for focusing charged particle beams.[5] We saw in Section 6.1 that an ideal quadrupole requires an infinitely long hyperbolic iron surface. A common method for terminating the iron boundary is to use symmetric cutoff angles θ_1, as shown for half of a symmetric pole in Figure 6.9.[6] The surface at the cutoff angles proceeds outwards along a radius. The equation of the hyperbolic surface relative to the centerline of the pole is
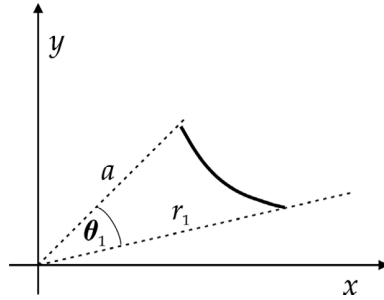
$$r^2 \cos 2\theta = a^2,$$

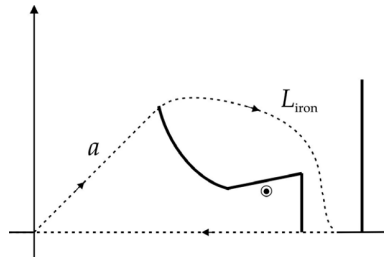Figure 6.9 Cutoff angle θ_1 for the iron surface in a quadrupole magnet.

Figure 6.10 Loop through the quadrupole.

where a is the radius to the center of the pole. The cutoff angle θ_1 can be selected to be ~27° in order to eliminate the first allowed error multipole B_6. In this case, the radius to the cutoff point is given by

$$\frac{r_1}{a} \simeq 1.12.$$

The choice of the angle θ_1 also determines the amount of space available for the conductor. Excitation of the iron poles by the conductor can be determined by using the Ampère law around the path shown in Figure 6.10.

$$NI \simeq \int_0^a \frac{B(r)}{\mu_0}\, dr + \frac{B_0 L_{iron}}{\mu}.$$

The contribution from the path in the iron may be neglected since $\mu_r \gg 1$. The contribution for the path along the x axis vanishes because the field is perpendicular to the path. Thus we have,

$$NI \simeq \int_0^a \frac{gr}{\mu_0}\, dr$$
$$= \frac{ga^2}{2\mu_0},$$

where *NI* is the amp-turns around a pole and *g* is the quadrupole field gradient. Thus the gradient is given by

$$g = \frac{2\mu_0 NI}{a^2} \tag{6.5}$$

and the pole tip field is

$$\begin{aligned} B_{pole} &= ga \\ &= \frac{2\mu_0 NI}{a}. \end{aligned} \tag{6.6}$$

Saturation in the iron affects the area near the conductor first.

Figure 6.11 shows a POISSON model[3] of a quadrupole with hyperbolic pole pieces. The figure shows 1/8 of the symmetric cross-section. The 45° boundary splits one of the four poles in half. The region in the vicinity of the origin is the open aperture. The rectangular box on the side of the pole for *x* ~14 to 26 cm is the conductor, which wraps around the pole and returns on the opposite side of the symmetric half pole piece. The pole piece is part of the iron yoke that provides a flux path to the symmetric adjacent pole.

High-field dipoles and quadrupoles require pole piece materials with a large value for the saturation magnetic flux density. A number of soft magnetic materials with large B_{sat} are listed in Table 6.2. Also listed are the initial and peak values for the permeability and the coercivity. The resistivity of the material is important for considerations of eddy current losses in time-varying operations.

Quadrupoles have also been constructed by approximating the hyperbolic surface with a circular cylinder.[6] Consider a circle tangent to the hyperbola at the center of the pole, as shown in Figure 6.12. The circular surface is continued out to a cut-off angle θ_1 with respect to the center of the pole and then extends outward along a radius. Let *a* be the shortest distance from the center of the magnet to the pole and *R* be the radius of curvature of the circle, which is centered at *C*. Then

$$\begin{aligned} R &= R \sin \theta_1 + a \sin \theta_1 \\ &= \frac{a \sin \theta_1}{1 - \sin \theta_1}. \end{aligned}$$

The radius of the cutoff point is

$$r_1 = (R + a)\cos \theta_1.$$

---

[3] This model is an example file that is part of the POISSON code distribution.

Table 6.2 *Magnetic alloys with large B_{sat} [9]*

Alloy	Composition[1]	B_{sat} [T]	Initial μ_r	Max μ_r	H_c [Oe][2]	ρ_e [$\mu\Omega$-cm]
	35Co,1Cr	2.42	650	10,000	0.63	20
Supermendur	49Co,2 V	2.40	800	70,000	0.23	40
Vanadium permendur	49Co,2 V	2.35	800	6,000	2.20	40
Iron		2.14	150	5,000	1.00	10
Silicon steel	0.5Si	2.05	280	3,000	0.90	28
silicon steel	3Si	2.01	290	8,000	0.70	47
grain-oriented Si steel	3Si	2.01	1,400	50,000	0.09	50

[1] In percent, balance is Fe; [2] 1 Oe = 1 10^{-4} T / μ_0.
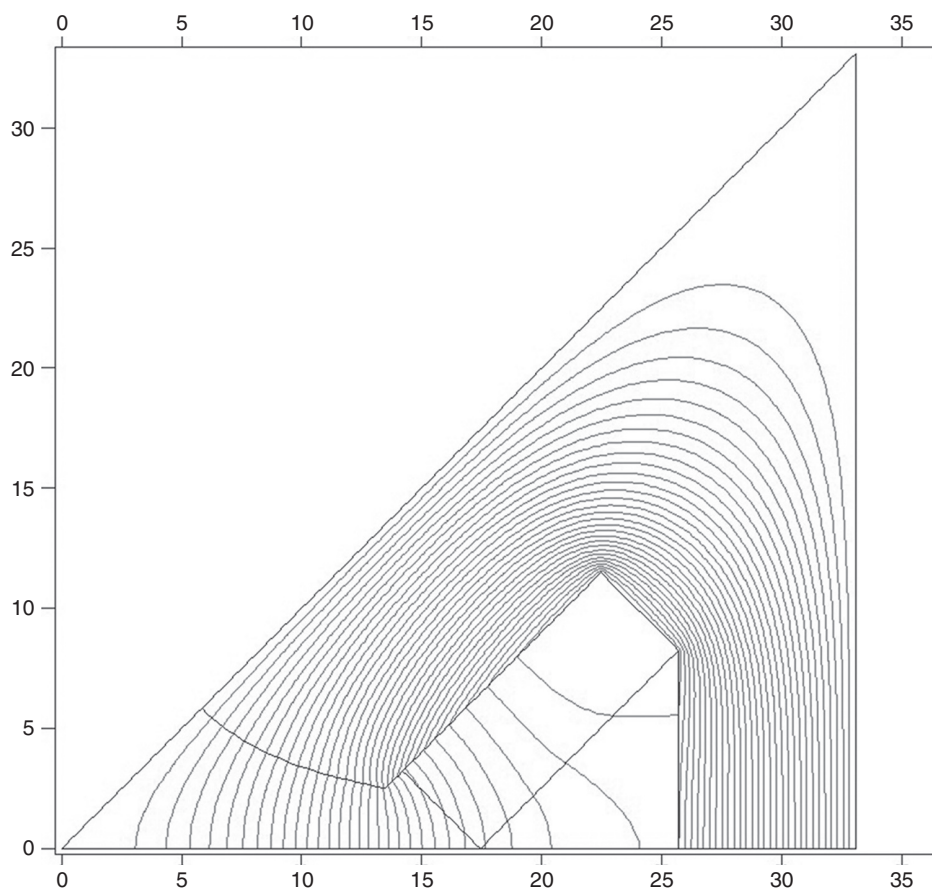

Figure 6.11 POISSON model of a quadrupole with hyperbolic pole pieces. Dimensions are in centimeters.
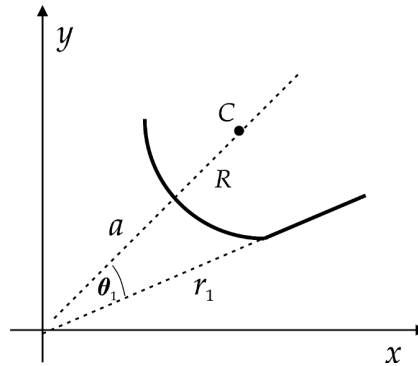
Figure 6.12 Quadrupole magnet with circular iron surface.

One solution to these equations, which makes the first allowed multipole harmonic $B_6 = 0$, is

$$\theta_1 = 31.5°$$

$$\frac{r_1}{a} = 1.785$$

$$\frac{R}{a} = 1.094.$$

Conformal mapping techniques have been used to simplify the design of quadrupoles and higher order multipole magnets.[10] The desired higher-order multipole is mapped to a dipole geometry, where it is easier to understand what effects proposed modifications make to the field in the useful aperture. It is also possible to numerically determine the field quality in the higher multipole aperture more accurately by computing the multipole coefficients in the transformed geometry.

References

[1] J. Tanabe, *Iron-Dominated Electromagnets*, World Scientific, 2005.
[2] T. Zickler, Basic design and engineering of normal-conducting, iron-dominated electromagnets, in *Proc. CERN Accelerator School on Magnets*, Bruges, Belgium, CERN-2010-004, June 2009, p. 65.
[3] K. Halbach, First order perturbation effects in iron dominated two dimensional symmetrical magnets, *Nuc. Instr. Meth.* 74:147, 1969.
[4] K. Halbach, Fields and first order perturbation effects in two dimensional conductor dominated magnets, *Nuc. Instr. Meth.* 78:185, 1970.
[5] A. Banford, *The Transport of Charged Particle Beams*, Spon Ltd., 1966, p. 81–84, 100–103.
[6] G. Parzen, Magnetic Fields for Transporting Charged Beams, Brookhaven National Laboratory Report 50536, 1976.

[7] G. Fischer, Iron-dominated magnets, *AIP Conf. Proc.* 153:1147–1151, 1987.

[8] P. Walstrom, Dipole magnet field models based on a conformal map, *Phys. Rev.-Spec. Top. Accel. Beams* 15:102401, 2012.

[9] Magnetically soft materials, *American Society for Metals (ASM) Handbook*, vol. 2, 1990, p. 761–781.

[10] K. Halbach, Application of conformal mapping to evaluation and design of magnets containing iron with nonlinear $B(H)$ characteristics, *Nuc. Instr. Meth.* 64:278, 1968.